https://doi.org/10.5194/nhess-2019-295
Preprint. Discussion started: 28 November 2019
© Author(s) 2019. CC BY 4.0 License.

Natural Hazards and Earth System Sciences
Discussions

The spatial-temporal total friction coefficient of the fault viewed from the seismo-electromagnetic theory.

Patricio Venegas-Aravena (1, 2), Enrique G. Cordaro (2, 3), David Laroze (4).

(1) Department of Structural and Geotechnical Engineering, School of Engineering, Pontificia Universidad Católica de Chile, Vicuña Mackenna 4860, Macul, Santiago, Chile.
(2) Cosmic Radiation Observatories, University of Chile, Casilla 487-3, Santiago, Chile
(3) Facultad de Ingeniería, Universidad Autónoma de Chile, Pedro de Valdivia 425, Santiago, Chile.
(4) Instituto de Alta Investigación, CEDENNA, Universidad de Tarapacá, Casilla 7D, Arica, Chile.

Author: P. Venegas-Aravena: plvenegas@uc.cl
Co-author: E. G. Cordaro: ecordaro@dfi.uchile.cl
Co-author: D. Laroze: dlarozen@uta.cl

Abstract

Recently, it has been shown theoretically how the lithospheric stress changes could be linked with magnetic anomalies, frequencies, spatial distribution and the magnetic-moment magnitude relation using the electrification of microfractures in the semi brittle-plastic rock regimen [Venegas-Aravena *et al.* Nat. Hazards Earth Syst. Sci. **19**, 1639 – 1651 (2019)]. However, this Seismo-electromagnetic Theory still has not shown any relation, approach or changes in the fault's properties in order to be linked with the beginning of seismic rupture process itself. In this work we show the first and simple theoretical approach to one of the key parameters for seismic ruptures as is the friction coefficient and the stress drop. We use sigmoidal stress changes in the non-elastic regimen within lithosphere described before to figure out the temporal changes in frictional properties of faults. We also use a long term friction coefficient approximation that can depend on the fault dip angle, four parameters that weight the first and second stress derivative, the spatial distribution of the non-constant stress changes and the stress drop. It is found that the friction coefficient is not constant in time and evolve previous and after the earthquake occurs regardless of the (non-zero) weight used. When we use a dip angle close to 30 degrees and the contribution of the second derivative is more significant than the first derivative, the friction coefficient increase previous the earthquake. Then, the earthquake occurs and the friction drop. Finally, the friction coefficient increases and decreases after the earthquake. When there is no contribution of stress changes in the semi brittle-plastic regimen, no changes are expected in the friction coefficient.

Keywords: Seismo-electromagnetic Theory, Friction coefficient, Magnetism, Earthquakes, LAIC effect.

1.- Introduction

During recent years, several works have appeared in different magnetic and ionospheric measurements that seem related to earthquakes. These measurements are part of the lithosphere-atmosphere-ionosphere-coupling effect (or LAIC effect) (e.g. De Santis et al., 2019a). Some researchers have shown co-seismic magnetic variations during some earthquakes (e.g. Utada et al. (2011) during Tohoku 2011 earthquake). Others researches have been focus on the oscillation frequency ($\mu Hz - kHz$ range) of magnetic field previous the occurrence of some earthquakes (Schekotov and Hayakawa, 2015; Cordaro et al., 2018; Potirakis et al., 2018a, b, among other). The magnetic anomalies have also been widely studied. For instance, De Santis et al. (2019b) have recently found an increase in the amount of daily magnetic

https://doi.org/10.5194/nhess-2019-295
Preprint. Discussion started: 28 November 2019
© Author(s) 2019. CC BY 4.0 License.

Natural Hazards and Earth System Sciences
Discussions

anomalies previous 12 earthquakes between 2014 and 2016. This increase also was found by other researchers (e.g. Marchetti and Akhoondzadeh (2018)).

On the other hand, experiments using rocks samples suffering fast changes on the uniaxial stress create microfractures, the displacement of dislocations and electrification in the semi brittle-plastic rock regimen (e.g. Anastasiadis et al., 2004). This physical mechanism of rock electrification is described mathematically by The Motion of Charged Edge Dislocations (MCD) model (e.g. see Vallianatos and Tzanis (1998) or Vallianatos and Tzanis (2003) for a comprehensive derivation of MCD model). This model seems to be a plausible electromechanical mechanism that could explain the magnetic measurements. Because of that Venegas-Aravena et al. (2019) developed a Seismo-electromagnetic Theory based on experimental microcracks and stress changes. This theory showed how the fractal nature of the cracks could explain the magnetic frequency range, the co-seismic magnetic field and the conditions for generating magnetic anomalies. However, this theory (in addition to others, e.g. Freund, 2003, De Santis et al., 2019a, among others) does not explain any change on the parameters that control the generation of seismic ruptures using magnetic measurements. This lack of knowledge makes the complete link between sesimo-electromagnetism and classical seismology impossible. In this work, we approach this link using one of the key points that control seismic rupture and slip on the fault: friction force and stress drop. During this work we use the tectonic geometry and stress drop of Maule 2010 Mw8.8 earthquake in order to base, develop and compare our analysis. Using this, in section 2 we develop the topic of friction coefficient adding the brittle-plastic stress changes contribution to the usual elastic stress. In section 3 we discuss the temporal changes of the brittle-plastic friction and the first implications of its spatial distribution on the fault and lithosphere. In section 4 is shown the stress drop in terms of the co-seismic magnetic field. The spatial-temporal friction coefficient along the fault is studied by adding the elastic stress drop. The Gutenberg-Richter's law is also written in terms of the semi brittle-plastic shear stress in section 5. The rupture time is discussed in section 6. Finally, the discussion and conclusion are shown in section 7.

2.- Friction coefficient in the brittle-plastic regimen

The standard friction force can be understood as the complex dissipation of mechanical energy in the form of plastic or elastic deformation of asperities (mechanical interaction), thermal dissipation (heat) and the adhesion (interatomic interaction) of two sliding surfaces (e.g. Sun and Mosleh, 1994). When we consider a particular contact area between two dry surfaces, the static friction coefficient μ that describes this interaction can be written approximately as the ratio of shear τ and normal N stress (load) as show Equation (1) (e.g. Byerlee, 1978, Chen, 2014, and references therein).

$$\mu = \frac{\tau}{N}. \qquad (1)$$

The static friction coefficient μ can give some information about the contact behavior. For instance, μ tend to be high when the contact area is increased due to the surface's plastic deformation (e.g. Chen, 2014). If we also consider the pure plastic regimen, we can add a small plastic shear stress ($\delta\tau_{plastic}$) and a small plastic normal stress ($\delta N_{plastic}$) contribution in Equation (1) leading to the following expressions:

$$\tau = \tau_{elastic} + \delta\tau_{plastic}. \qquad (2)$$

$$N = N_{elastic} + \delta N_{plastic}. \qquad (3)$$

https://doi.org/10.5194/nhess-2019-295
Preprint. Discussion started: 28 November 2019
© Author(s) 2019. CC BY 4.0 License.

Natural Hazards and Earth System Sciences
Discussions

If we do not consider the pure plastic effects, the plastic contribution is vanished and the ratio of $\tau_{elastic}$ and $N_{elastic}$ describe the usual (non-linear) friction behaviors that occur during the complete frictional cycle: Pre-Sliding (increase of friction coefficient when there is no-apparent or residual displacement), Gross-Sliding (observable displacement and decrease of friction coefficient) and Healing (friction coefficient recovery) (e.g., Parlitz et al., 2004, Marone and Saffer, 2015, Papangelo et al., 2015, and references therein).

On the other hand, Venegas-Aravena et al. (2019) state that the electrification within rocks is mainly due to a non-constant stress change during the semi brittle-plastic transition. This means that the temporal changes of the semi brittle-plastic stress ($\delta\sigma_{sbp}$) rules the total plastic stress ($\delta\sigma_{pastic}$). Thus, it implies that the plastic shear and normal stress can be written in terms of a linear combination of the temporal changes of $\delta\sigma_{sbp}$ as show Equation (4) and (5).

$$\delta\tau_{plastic} = k_1\delta\tau_{sbp} + k_2\delta^2\tau_{sbp} + o(\delta^2\tau) = k_1\,\dot{\tau}_{sbp}\delta t + k_2\,\ddot{\tau}_{sbp}(\delta t)^2 + o((\delta t)^2), \qquad (4)$$

$$\delta N_{plastic} = k_3\delta N_{sbp} + k_4\delta^2 N_{sbp} + o(\delta^2 N) = k_3\,\dot{N}_{sbp}\,\delta t + k_4\,\ddot{N}_{sbp}(\delta t)^2 + o((\delta t)^2), \qquad (5)$$

where $k_1,\ k_2,\ k_3$ and k_4 are dimensionless constants to determine, δt and $(\delta t)^2$ are the temporal delta from the first and second order time contribution. The temporal variations of the shear and normal semi brittle-plastic stress contributions are $\dot{\tau}_{sbp}, \ddot{\tau}_{sbp}, \dot{N}_{sbp}$ and $\ddot{N}_{sbp}$ respectively. The expansion in Equations (4) and (5) are convenient because they allow studying the plastic contribution as a sum of stresses that depend on time. This is relevant because the seismic-electromagnetic theory seeks to relate the temporal variable of earthquake prediction and stress within the lithosphere. Here and after we refer to the semi brittle-plastic stress just as the uniaxial stress σ.

It is possible to relate this shear, and the normal stresses from Equations (4) – (5) with the uniaxial stress using the geometry shown in Figure 1. In this Figure, it is possible to observe a simple schematic representation of the lithosphere under uniaxial stress change $d\boldsymbol{\sigma}/dt$ in the presence of a fault with static friction coefficient μ and a dip angle of 30 degrees. We can write this uniaxial stress change in terms of the dip angle θ, normal and tangential direction (in red on Figure 1) of the fault, as shown in the following expression

$$\frac{d\boldsymbol{\sigma}}{dt} = \frac{d\sigma}{dt}(-\sin\theta\,\hat{N} + \cos\theta\,\hat{\tau}), \qquad (6)$$

where $d\sigma/dt$ corresponds to the magnitude of uniaxial temporal stress change. Using this, we can write the brittle-plastic stress contributions in term of uniaxial stress change as:

$$\dot{N} = -\frac{d\sigma}{dt}\sin\theta. \qquad (7)$$

$$\dot{\tau} = \frac{d\sigma}{dt}\cos\theta. \qquad (8)$$

Replacing the Equations (2) – (8) in Equation (1), and considering a second-order linear combination, we can obtain the static friction coefficient as a function of time, the fault angle and the semi brittle-plastics changes within lithosphere given by:

$$\mu(t) \approx \frac{\tau_0 + (k_1\,\dot{\sigma} + k_2\,\ddot{\sigma}\delta t)\cos\theta\,\delta t}{N_0 - (k_3\dot{\sigma} + k_4\,\ddot{\sigma}\,\delta t)\sin\theta\,\delta t}, \qquad (9)$$

https://doi.org/10.5194/nhess-2019-295
Preprint. Discussion started: 28 November 2019
© Author(s) 2019. CC BY 4.0 License.

Natural Hazards and Earth System Sciences
Discussions

where the dots above σ mean first and second temporal derivative of uniaxial stress. According to Venegas-Aravena et al. (2019), the temporal stress change $\dot{\sigma}$ has sigmoidal shape, which can be defined as $\dot{\sigma}(t) = a/(b + e^{(t0-t)*w})$, where a, b, w and t_0 are constants. In Figure 2 we can see a dimensionless shape of $\dot{\sigma}$ and $\ddot{\sigma}$ as a function of time when we use $a = b = w = 1$ and $t_0 = 10$. According to De Santis et al. (2019b), most of the earthquakes recorded occurred close to the center of the Figure 2, which is when $t_{EQ} = t_0$. For instance, Marchetti and Akhoondzadeh (2018) shown that the Mexico earthquake Mw8.2 occurred after this time ($t_{EQ} > t_0$). They also use daily values of magnetic anomalies ($B \propto \frac{d\sigma}{dt}$, which comes directly from the experimental equation: $I = \alpha_0 \frac{d\sigma}{dt}$, where I is the electric current and α_0 is a constant of proportionality (e.g., Vallianatos, F. and Triantis and references therein)), thus $\delta t = 1\ day = 86400\ s$.

Let us now, to figure out the values of constants of Equation (9). First, the dip or subduction angle θ is needed. According to Maksymowicz (2015), this angle is close to 20 degrees at the depth ($\sim 30\ km$) and location (35°54′32″S, 72°43′59″W) of Maule 2010 earthquake. Maksymowicz (2015) claim that the static friction coefficient in the Chilean convergent margin is close $\mu_{ch} \approx 0.5$. Lamb (2006) calculate that the initial value of τ_0 is 15.4 MPa (constant) in southern Chile. Using μ_{ch}, it is expected that N_0 should be close to 30.8 MPa (constant).

On the other hand, rock experiments show that the values of $\dot{\sigma}$ are close to 1 MP/s (e. g. Saltas et al., (2018)). This implies that $|k_1|$ and $|k_3|$ must be close to $\sim 10^{-4}$, in order to balance the δt factor. The values of k_2 and k_4 must be equal or lesser than $\sim 10^{-9}$. Otherwise, the values of friction coefficient would be greater than 1. If we consider an initial increase of the normal stress, the sign of the constants should be negative for k_3, k_4 and positive for k_1, k_2. In Figure 3 we can see how the friction coefficient changes in time, when using values of k_1 and k_3 described above, and different values of k_2 and k_4 (second order contribution). When we use values of k_2 and k_4 similar to $\sim 10^{-9}$, it's possible to observe how the friction decreases after the earthquake. Furthermore, it's important to note that the earthquake does not occur when the friction has its maximum value, but occurs close to it. When we use values of k_2 and k_4 similar or lesser than $\sim 10^{-10}$ the contribution of $\ddot{\sigma}$ in Equation (9) is vanished.

Another critical point is related to the differential time. For instance, when we consider $\delta t \leq 1\ s$, implies that the semi brittle-plastic stress term vanishes due to the values of the parameters and the usual friction are recovered. This fact is especially notable because the semi brittle-plastic contribution to the friction coefficient seems to be relevant only during long periods. In other words, the friction coefficient of Equation (9) could be view as a generalization of the standard friction when long periods are considered.

3.- Spatial distribution of stress changes and friction

In the previous section it was possible to link the friction coefficient to the semi brittle-plastic regimen that generates microcracks and electrification within the rocks. However, this phenomena seems not to occur everywhere. For instance, Dobrovolsky et al. (1979) described a specific "preparation zone" required close to the future hypocenter in order to accumulate sufficient stress to triggers the earthquake. This criterion has been widely used by modern researchers to establish a limit where the magnetic measurements can be associated to earthquakes (e.g. De Santis et al., 2019a, De Santis et al., 2019b). In other words, this phenomena is local. However, if this is applied, a variation of the friction coefficient related to the rock electrification phenomena close to the fault would be expected, while a friction variation outside zones of semi brittle-plastic influence would not be.

https://doi.org/10.5194/nhess-2019-295
Preprint. Discussion started: 28 November 2019
© Author(s) 2019. CC BY 4.0 License.

Natural Hazards and Earth System Sciences
Discussions

In order to consider this feature, we can add a spatial function to the uniaxial stress as $\bar{\sigma}(x,t) = \gamma(x)\sigma(t)$ (for simplicity we choose only the x direction). Where $\sigma(t)$ correspond to the same uniaxial stress considered before and $\gamma(x)$ is the dimensionless spatial distribution parallel to the fault (see the coordinate system in Figure 4). Furthermore, the values of $\gamma(x)$ must be different when constant and non-constant stress changes are considered. With this, we can re-write Equation (9) as:

$$\bar{\mu}\,(x,t) \approx \frac{\tau_0 + \gamma(k_1\,\dot{\sigma} + k_2\,\ddot{\sigma}\delta t\,)\cos\theta\,\delta t}{N_0 - \gamma(k_3\dot{\sigma} + k_4\,\ddot{\sigma}\,\delta t)\sin\theta\,\delta t}. \qquad (10)$$

Furthermore, after straightforward calculations, we can calculate the gradient of the friction coefficient along the fault using Equation (10) as:

$$\nabla\bar{\mu}(x,t) = \gamma'\,\frac{AN_0 + B\tau_0}{(N_0 - \gamma B)^2} = \gamma'\frac{\alpha\,\dot{\sigma}\delta t + \beta\,\ddot{\sigma}\delta t^2}{(N_0 - \gamma B)^2}, \qquad (11)$$

where $A = (k_1\,\dot{\sigma} + k_2\,\ddot{\sigma}\delta t\,)\cos\theta\,\delta t,\ B = (k_3\dot{\sigma} + k_4\,\ddot{\sigma}\,\delta t)\sin\theta\,\delta t,\ \alpha = N_0k_1\cos\theta + \tau_0k_3\sin\theta$ and $\beta = N_0k_2\cos\theta + \tau_0k_4\sin\theta$. Equation (10) and (11) imply that if we distribute the constant and non-constant temporal stress change in a non-uniform manner along the fault, then, it could be said that this phenomenon is local. This can be understood using the example of Figure 4: The Figure 4a shows a blue area of length L where it is applied a non-constant temporal stress change. Then, it is expected that the fault suffers a change in the friction coefficient inside the projected gray area (Figure 4b). On the other hand, if we consider that there is a constant stress change outside the area of length L, (Figure 4c), then we would not expect any change in the friction coefficient (Figure 4d). It's important to keep in mind that the entire fault suffered from stress accumulation during the entire example. However, only the grey area could be affected by the friction change. This example also shows that the temporal friction changes are restricted only to a specific area (grey area) on the fault. Hence, must exist a non-zero friction coefficient gradient on the fault to have a local phenomenon ($\nabla\,\bar{\mu} \neq 0 \Leftrightarrow Local$).

The example of Figure 4 reveals why it is expected that magnetic measurements are not a global phenomenon and also validate the locality criteria in terms of fault properties. Furthermore, the spatial distribution of magnetic measurements is expected to be comparable to the spatial length of change in the friction coefficient due to the dependency of $\gamma(x)$ in Equation (10). That is the larger detection area of magnetic anomalies, the higher the area where fault friction is changing. In addition, Venegas-Aravena et al. (2019) describe how the uniaxial stress change implies a change in the b-value of the Gutenberg-Richter Law. It also implies that a significant earthquake is needed in order to satisfy this change in the Gutenberg-Richter Law. Hence, the greater magnitude (and amount of earthquakes) expected could be related to the changes in the frictional coefficient within localized areas on the fault. However, changes in the friction coefficient do not directly implies the earthquakes generation itself.

4.- Stress drop and Total friction coefficient: Spatial-temporal behavior

Up to this moment, no changes in the elastic stresses have been considered in Equation (10). Because of that, this section is studies one of the elastic parameters that are involved in the seismic rupture process: the stress drop $\Delta\tau$. This parameter is one of the most relevant because it show the shear stress differences prior to and after the earthquake event within the fault rupture area (e.g. Aki, 1966). Furthermore, it can be also linked with the seismic waves radiated (through the corner frequency of waves) and the seismic moment M_0 (e.g. Eshelby, 1957, Brune, 1970, Baltay et al., 2011, and references therein). If we consider

https://doi.org/10.5194/nhess-2019-295
Preprint. Discussion started: 28 November 2019
© Author(s) 2019. CC BY 4.0 License.

Natural Hazards and Earth System Sciences
Discussions

a circular rupture area with radius d_{crack}, the stress drop $\Delta\tau$ is linked with the seismic moment M_0 through the following equation (Eshelby, 1957).

$$\Delta\tau = \frac{7}{16}\frac{M_0}{d_{crack}^3}. \qquad (12)$$

On the other hand, the seismic moment M_0 and moment magnitude Mw in terms of the co-seismic magnetic field can be related. Hence, the seismic moment is given by:

$$M_0 \approx \mu_{sm}\frac{B_{cs}r^2}{\mu_m J}\frac{(3-D)}{D(D-2)}\left(l_{min}^{2-D}\right)\left(l_{max}^{D-3}\right)d, \qquad (13)$$

where μ_{sm} is the shear modulus, d the average slip, D fractal dimension of rock, B_{cs} the co-seismic magnetic field, J corresponds to the total electric current density, μ_m is the magnetic permeability of the medium, r the distance to the fault, l_{max} and l_{min} are the radius of the circular rupture area and the smallest microcrack length, respectively. The circular rupture is calculated using $l_{max} = \sqrt{S/\pi}$, where S corresponds to the total rupture area.

In this case, the rupture geometry is circular in both formulations, thus, $d_{crack} = l_{max}$. Replacing this into Equation (13) and Equation (12):

$$\Delta\tau \approx \frac{7}{16}\,\mu_{sm}\frac{B_{cs}r^2}{\mu_m J}\frac{(3-D)}{D(D-2)}\left(l_{min}^{2-D}\right)\left(l_{max}^{D-6}\right)d. \qquad (14)$$

Equation (14) relates the stress drop with the co-seismic magnetic measurements, seismic rupture, and the electrical and mechanical properties of rocks (lithosphere). We can use the data from the Maule earthquake in order to contrast the result of Equation (14) with those found by other researchers. If we use the fault values: $\mu_{sm} = 3.3 \times 10^{10}\ Pa$, $d = 4\ m$ and $S = 450 \times 120\ \text{km}^2$ (Vigny et al., 2011; Yue et al., 2014), the granite rock and brittle properties: $\mu_m = 13.5 \times 10^{-7}\ NA^{-2}$ (Scott, 1983), $J = 5 \times 10^{-6}\ Am^{-2}$ (Tzanis and Vallianatos, 2002), $l_{min} = 10^{-3}\ m$ (Shah, 2011) and $D = 2.6$ (Turcotte, 1997). The magnetic data $B_{cs} \approx 0.1\ nT$ at $r \approx 250$ km (Figure 5 in Venegas-Aravena et al. (2019)), we obtain a stress drop $\Delta\tau \approx 3.4\ MPa$. This result is close similar to the result of Luttrell et al. (2011) (4 MPa). Using this, we can calculate the elastic shear stress as:

$$\tau_{elastic} = \tau_0 - \gamma_2\Delta\tau H(t - t_0), \qquad (15)$$

where $H(t - t_0)$ correspond to the step function centered at t_0 (the time when the earthquake occurs) and γ_2 is a second step function that represents the fault area where exist the stress drop. This means that if $\gamma_2 = 0$ if is considered a point outside the rupture area, and $\gamma_2 = 1$ if the point is within the rupture area. Adding this result to Equation (10), we are able to calculate the total friction coefficient $\bar{\mu}_T$ of fault as:

$$\bar{\mu}_T\,(x,t) \approx \frac{\tau_0 - \gamma_2\Delta\tau H(t-t_0) + \gamma\,(k_1\,\dot{\sigma} + k_2\,\ddot{\sigma}\delta t\,)\cos\theta\,\delta t}{N_0 - \gamma\,(k_3\dot{\sigma} + k_4\,\ddot{\sigma}\,\delta t)\sin\theta\,\delta t}. \qquad (16)$$

This total friction coefficient $\bar{\mu}_T$ is especially relevant because of the dependence of the co-seismic magnetic measurements B_{cs} (through the stress drop $\Delta\tau$) and the magnetic anomalies (through the relation $B \propto \dot{\sigma}$). Furthermore, Equation (16) explains the spatial distribution of friction along the fault in addition to the time variations. In this Equation, it is also clear that the spatial changes of friction (represented by γ) are not necessarily related to the seismic rupture area (represented by γ_2). However, in the case that if they are really related, it is expected that γ_2 would be a function of γ (or vice versa). That is $\gamma_2 = \gamma_2(\gamma(x))$. The general case of total friction coefficient gradient can be written as:

$$\nabla\bar{\mu}_T = \nabla\bar{\mu} + \Delta\tau H(t - t_0)\,\Gamma(\gamma,\gamma_2), \qquad (17)$$

https://doi.org/10.5194/nhess-2019-295
Preprint. Discussion started: 28 November 2019
© Author(s) 2019. CC BY 4.0 License.

Natural Hazards and Earth System Sciences
Discussions

where $\Gamma(\gamma,\gamma_2)=\frac{1}{(N_0-\gamma B)^2}\,[\gamma_2'(\gamma B-N_0)-\gamma'\gamma_2 B]$, $\nabla\bar{\mu}$ is the friction gradient defined in Equation (11), and the same definition of A and B are used. The second term of Equation (17) implies that more complex spatial friction distribution on the fault is expected after the earthquake. When no brittle-plastic contribution is considered ($\gamma=0$), the friction is only proportional to the gradient of fault rupture distribution ($\nabla\bar{\mu}_T=-\Delta\tau H(t-t_0)\gamma_2'/N_0$). When $\gamma_2\approx\gamma$, the two terms of the Total Friction Coefficient will be proportional to the spatial distribution gradient ($\nabla\bar{\mu}_T\propto\gamma'$). If the earthquake does not occur, the second term vanishes and the Equation (11) is recovered.

On the other hand, if we consider one point affected by the rupture area, and the same values needed to create the Figure 3, we can calculate the shape of the total friction coefficient as is shown in Figure 5. The tree cases show the increase of friction coefficient prior the earthquake, and in the tree cases the friction reach it maximum values before the earthquake (t=10). The decrease is due the stress drop influence calculated using the co-seismic magnetic field B_{cs}. After the earthquake, in none of the cases, the friction is completely recovered to values instantly before the earthquake.

Furthermore, it is also possible to compare the temporal behavior of the friction coefficient in terms of the fault point choose. For instance, in Figure 6 (above) is shown the different friction behavior expected if we consider the Total friction coefficient. There it is also pointed out the seismic rupture (blue area) influence in terms of the stress drop. This stress drop is not expected out the seismic rupture, however, still is possible to observe differences in the friction behavior at the point close to the rupture (yellow area) in the case $\gamma_2\neq\gamma$. In Figure 6 (bottom), the standard friction drop is expected at the rupture area. However, a non-measurable change in friction is observed prior to the earthquake.

We can quantify this analysis using two different distribution of γ and γ_2. For instance, in Figure 7 is shown the double-sigmoidal distribution for γ and γ_2(black and red curves respectively) along the fault x-direction (of total length $2x_{half}$). The dimensionless distribution is defined as a combination of sigmoidal function used in the section 2 as:

$$\gamma(x),\gamma_2(x)=\begin{cases}\dfrac{a}{b-e^{(x_0-x)*w}}, & x<x_{half}\\ 1-\dfrac{a}{b-e^{(x_0+L-x)*w}}, & x\geq x_{half}\end{cases}. \qquad (18)$$

If we consider $a=b=1$ and $x_{half}=10$ in both distributions, and $x_0=5, L=10$ and $w=1$ for γ and $x_0=8,\ L=4$ and $w=10$ for γ_2, we can create the two distributions of Figure 7. These values show the same scenario discuss in Figure 6. That is a rupture length ($L=4$ in γ_2 represent the x-direction of the red area in Figure 6) lesser than the friction coefficient influenced by semi brittle-plastic stress (here $L=10$ in γ represent the x-direction of the yellow area in Figure 6). Using both sets of values, those used in the stress drop (Equation (14)) and also the same k-parameters used in Equation (9), it is possible to calculate the total friction coefficient (Equation (16)) as shown the Figure 8 (case $k_2=\ k_4=10^{-9}$). At time t = 0, no friction changes occur ($\bar{\mu}_T=0.5$). However, the friction increase begins close to t=5, where the spatial distribution γ is initially defined as non-zero ($x\in[5,15]$). The friction increases up to t=10, the time where the earthquake occurs. The earthquake rupture length is shown as a sudden friction decrease ($x\in[8,12]$) from 0.76 to 0.67. In the zone immediately close to the rupture, the friction increases even more up to the maximum values (0.77), while the rupture section decreases the friction. After this time (t~12), the rupture and surrounding section have a friction decrease.

The case of $k_2=\ k_4=10^{-10}$ is shown in Figure 9. The rupture is shown as a blue area at t=10 in section $x\in[8,12]$. At this time and location it is possible to observe that friction decreases to similar initial values (~0.5). The friction of this rupture section increase after the earthquake up to ~0.6. On the

https://doi.org/10.5194/nhess-2019-295
Preprint. Discussion started: 28 November 2019
© Author(s) 2019. CC BY 4.0 License.

Natural Hazards and Earth System Sciences
Discussions

other hand, the rupture's surrounding section increases up to the maximum values (~0.7). Despite of this, the initial (t=0) and final (t=20) friction values are almost similar for both cases. For instance, the rupture area has values close to 0.6 in Figures 8 and 9. The surrounding rupture section has values close to 0.69 in both cases and the section away from the rupture (close to x=0 and x=20) always has the same initial value (0.5) in both cases. Besides, both cases exhibit a complex behavior after de earthquake occurs, as Equation (17) reveals.

On the other hand, when the semi brittle-plastic contribution is not considered, it implies that $\gamma = 0$. The result is shown in Figure 10 and is only observed the sudden friction decrease at t=10 (and $x \in [8, 12]$). Furthermore, not any other complex friction behavior is observed.

5.- The semi brittle-plastic Gutenberg-Richter law

A general expression for friction has been obtained in Equation (16). Moreover, it is possible to study the Gutenberg-Richter's law in this semi brittle-plastic context. This law establishes a relation between the number of earthquakes that exist in a region and the magnitude of them (Gutenberg and Richter, 1944). Mathematically, this link is written as: $\log N = a - b \times m$. Where N is the number of earthquakes with magnitude equal to or greater than m, and a and b are constants. However, the b-value of this law might evolve and not be constant on time. On the other hand, De Santis et al. (2011) determined an equation that relate the temporal evolution of b-value ($b = b(t)$) and the measure of the stress $H(t)$ of that region as $b(t) = b_{max}10^{-H(t)}$, where $b_{max} = e \log_{10} e$. This stress measurement $H(t)$ can be proportional to the real stress in the lithosphere (Venegas-Aravena et al., 2019). If we consider the total shear stress τ_T in the fault described by Equation (16), we can write:

$$b(t) = b_{max}10^{-k_0\tau_T}, \qquad (19)$$

where $\tau_T = \tau_0 - \gamma_2\Delta\tau H(t - t_0) + \gamma\,(k_1\,\dot{\sigma} + k_2\,\ddot{\sigma}\delta t\,)\cos\theta\,\delta t$ and k_0 is a constant in units of inverse stress. If we use the same values that were used to create Figure 5 ($k_2 = k_4 = 10^{-9}$), we can find the temporal evolution of the b-value (Figure 11a). Figure 11a shows a decrease in b-value until the earthquake occurs (t=10). Figure 11b shows the Gutenberg-Richter's law for three instants of time (and $k_0 = 0.01$, a=1): initial (t=0), prior to the earthquake (t=9) and final (t=20). This Figure shows how large earthquakes (Mw ~ 6) are not expected at the initial moment (blue line). However, just before the earthquake, an M8-class earthquake should be expected (green line). After the earthquake one would only expect earthquakes no greater than Mw ~ 7 to exist (red line). Figure 12a and 12b show the same previous case but considering $k_2 = k_4 = 10^{-10}$. In this case there are no differences between time, immediately before the earthquake (t=9) and at the end time (t=20). In addition, using these parameters ($k_2 = k_4 = 10^{-10}$), smaller magnitudes are reached than using $k_2 = k_4 = 10^{-9}$ (Mw~7 and Mw~8 respectively). This is why it is more likely to find earthquakes of greater magnitude when considering the contribution of $\ddot{\sigma}$ within analyzes.

6.- Rupture time t_0

In section 5 it was found that $k_2 = k_4 = 10^{-9}$ values were more adequate. Despite this, the Gutenberg-Richter law does not give us an approximate time $\boldsymbol{t_0}$ for the earthquake occurrences. If we look at Equation (16), the term $\boldsymbol{t_0}$ appears explicitly (step function). However, $\boldsymbol{t_0}$ appears only after the earthquake, so it is not possible to find $\boldsymbol{t_0}$ analytically before the rupture (using the rupture itself). This

https://doi.org/10.5194/nhess-2019-295
Preprint. Discussion started: 28 November 2019
© Author(s) 2019. CC BY 4.0 License.

Natural Hazards and Earth System Sciences
Discussions

means that we must find an approximate expression from other parameters. For example, if we consider the differential total friction coefficient $d\bar{\mu}_T$ it is possible to find approximate rupture time t_0. Figure 13 shows $d\bar{\mu}_T$ considering $\gamma_2 = \gamma = 1$, $k_2 = k_4 = 10^{-9}$ and $k_2 = k_4 = 10^{-10}$. When major earthquakes expected ($k_2 = k_4 = 10^{-9}$) are considered, the rupture occurs after the maximum value ($(d\bar{\mu}_T)_{MAX}$), when $d\bar{\mu}_T \approx \frac{1}{2}\,(d\bar{\mu}_T)_{MAX}$ (Figure 13 up). When $k_2, k_4 = 10^{-10}$, the rupture also occurs after the maximum value, different to the case in which $d\bar{\mu}_T \approx 0.9\,(d\bar{\mu}_T)_{MAX}$ (Figure 13 down). Considering these two cases within this theory, we can write that earthquakes occur after $(d\bar{\mu}_T)_{MAX}$ when the differential total friction coefficient decrease to $d\bar{\mu}_T \approx \mathrm{C}\,(d\bar{\mu}_T)_{MAX}$, where $C \in [0.5,\ 0.9]$.

On the other hand, the time between $d\bar{\mu}_T \approx (d\bar{\mu}_T)_{MAX}$ and $d\bar{\mu}_T \approx \mathrm{C}\,(d\bar{\mu}_T)_{MAX}$ can be represented as δ. This δ parameter increases when C decreases and viceversa, so δ is inversely proportional to C ($\delta \propto C^{-1}$). Then, we can write the general rupture time t_0 as:

$$t_0 \approx t_{\mathrm{C}\,(d\bar{\mu}_T)_{MAX}} = t_{(d\bar{\mu}_T)_{MAX}} + \delta, \quad t > t_{(d\bar{\mu}_T)_{MAX}}, \qquad (20)$$

where $t_{(d\bar{\mu}_T)_{MAX}}$ is the time when $d\bar{\mu}_T \approx (d\bar{\mu}_T)_{MAX}$. Note that the Equation (20) is only valid after the maximum value $(d\bar{\mu}_T)_{MAX}$ is reached. Equation (20) is general, however, considering the Gutenberg-Richter law, it would be expected that C values close to 0.5 are necessary to represent earthquakes of greater magnitude in this theory.

7.- Discussion and conclusions

In this work it was possible to relate one of the properties of the key faults to the magnetic measurements. Both stress drops and the semi brittle-plastic stress were linked to friction coefficient (on the fault) equation in terms of magnetic measurements (Equation (16)). One of the critical points of Equation (16) corresponds to the fact that the Total Friction Coefficient $\bar{\mu}_T(x,t)$ is entirely determined by the spatial distribution of the non-constant stress changes within the lithosphere. If the Seismo-electromagnetic theory is applied, it implies that the rupture process might be controlled by the non-constant stress changes that surround the fault and not entirely by the fault itself. In this scenario, the earthquakes might occur at places on the fault that are being affected by a continuous friction increase prior to rupture (this friction increase occur regardless of the values of k_2 and k_4 used). However, the Total Friction Coefficient depends on two different spatial distribution. The first one is associated with the uniaxial stress changes $\gamma(x)$ and the second one to the rupture area $\gamma_2(x)$. This two distribution are not necessarily correlated. In the case that both are comparable (that is: $|\gamma(x) - \gamma_2(x)| \approx 0$), it could mean that the lithosphere area affected by non-constant uniaxial stress changes could determine the earthquake magnitude and location before it occurs. This is $\gamma(x) \approx \gamma_2(x) \approx 0$ if x belong to sections where $\dot{\sigma} = cte$ and $\gamma(x), \gamma_2(x) \neq 0$ if $x \in L$, where L is the rupture length (places where $\dot{\sigma} \neq cte$). The seismic moment M_0 is proportional to this length L (Aki, 1966), and the seismic moment magnitude M_w depend on the seismic moment (Hanks and Kanamori, 1979), implying that the seismic moment magnitude could depend on the spatial distribution of the total friction coefficient increases. As the non-constant uniaxial stress changes also could create magnetic signals due the microcracks of rocks (Venegas-Aravena et al., 2019, and references therein), it is valid to say that a larger area of magnetic anomaly measurements could imply a larger earthquake. This is the locality (Dobrovolsky) criteria used by some researchers when they try to relate some electromagnetic measurements to earthquakes (e.g., De Santis et al., 2019a, and references therein). If in this case we also consider the initial time of friction increase (impending rupture time), the approximate magnitude, the approximate location and the approximate imminent time could be theoretically determined.

https://doi.org/10.5194/nhess-2019-295
Preprint. Discussion started: 28 November 2019
© Author(s) 2019. CC BY 4.0 License.

Natural Hazards and Earth System Sciences
Discussions

On the other hand, if $|\gamma(x) - \gamma_2(x)| \gg 0$ implies that the locality criteria does not hold anymore. Hence, the earthquakes occurrences should not be related to the non-constant stress changes and the magnetic measurements. Furthermore, this case also closes the possibility of a real earthquake prediction using this theoretical base. This case may also imply that the cumulative stress on the fault is not enough to generate a seismic rupture at any point on the fault (this is $\gamma_2(x) = 0$). This means that the semi brittle-plastic energy injected to the fault is lesser than the Fracture Energy G (The energy required to spread a rupture, e.g., Nielsen et al., 2016, and references therein). The last scenario could indicate that the stress changes are not a sufficient condition to the earthquake generation, however, it could be a necessary condition.

With respect to the size of earthquakes in this model, the section 5 revealed that earthquakes may have greater magnitudes when $k_2 = k_4 \approx 10^{-9}$. If we consider those values in Figure 5, we can see that the total friction coefficient is also higher. This is ~0.75 when $k_2 = k_4 \approx 10^{-9}$ and ~0.6 when $k_2 = k_4 \approx 10^{-10}$. This indicates that there could be also a correlation between the size of the earthquake and the total friction coefficient. Hence, the earthquake has a greater magnitude when there is a higher total friction coefficient (or shear stress τ). This means that $\gamma_2 = \gamma_2(\bar{\mu}_T)$, therefore, the rupture length L of Equation (18) is proportional to $\bar{\mu}_T$ (that is: $L = \alpha\bar{\mu}_T(t_0)$). Note that this is independent of the value of $|\gamma(x) - \gamma_2(x)|$, since it comes directly from the Gutenberg-Richter's law. However, in this case $\bar{\mu}_T$ is homogeneous, so more studies will be needed when it is not to calculate L.

Finally, this theoretical work has shown a possible mechanism that explains several magnetic measurements performed during the last years. Furthermore, it has also been possible to perform some studies that reveal the possible necessary conditions of the fault to trigger earthquakes in terms of the magnetic properties. Hence, future investigations of the LAIC effect community should also be focused on the lithospheric-fault dynamics as one of the main topics. When the lithosphere part of this effect would be understood, the others effects will have a strong theoretical base in order to perform measurements and/or any predictions.

Acknowledgments

In memory of Marcela Larenas Clerc (1960-2019). P.V.-A. acknowledges Patricia Aravena, Alejandro Venegas, Patricia Venegas and Richard Sandoval for outstanding support to carry out this work, and Valeria Becerra-Carreño for her scientific support. D. L. acknowledges partial financial support from Centers of excellence with BASAL/CONICYT financing, grant FB0807, CEDENNA.

https://doi.org/10.5194/nhess-2019-295
Preprint. Discussion started: 28 November 2019
© Author(s) 2019. CC BY 4.0 License.

Natural Hazards and Earth System Sciences
Discussions

References

Aki, K.: Generation and propagation of G waves from the Niigata earthquake of June 14, 1964. Part 2. Estimation of earthquake moment, released energy and stress-strain drop from G wave spectrum. Bulletin of the Earthquake Research Institute, 44: 73–88, 1966.

Anastasiadis, C., Triantis, D., Stavrakas, I. and Vallianatos, F.: Pressure Stimulated Currents (PSC) in marble samples. Ann. Geophys., 47, 1, pp. 21-28, 2004.

Baltay, A., Ide, S., Prieto, G. and Beroza, G.: Variability in earthquake stress drop and apparent stress. Geophysical Research Letters. VOL. 38, L06303, doi:10.1029/2011GL046698, 2011.

Brune, J. N.: Tectonic stress and the spectra of seismic shear waves from earthquakes, J. Geophys. Res., 75(26), 4997–5009, doi:10.1029/JB075i026p04997, 1970.

Byerlee, J.D.: Friction of Rocks. Pure and Applied Geophysics. 116 (4–5): 615–626. doi:10.1007/BF00876528, 1978.

Chen, G.S.: Fundamentals of contact mechanics and friction. Handbook of Friction-Vibration Interactions, 71–152. doi:10.1533/9780857094599.71, 2014.

Cordaro, E.G., Venegas, P. and Laroze, D.: Latitudinal variation rate of geomagnetic cutoff rigidity in the active Chilean convergent margin. Ann. Geophys., 36, 275–285, https://doi.org/10.5194/angeo-36-275-2018, 2018.

De Santis, A., Cianchini, G., Favali, P., Beranzoli, L., and Boschi, E.: The Gutenberg–Richter Law and Entropy of Earthquakes: Two Case Studies in Central Italy, B. Seismol. Soc. Am., 101, 1386–1395, https://doi.org/10.1785/0120090390, 2011.

De Santis, A., Abbattista, C., Alfonsi, L., Amoruso, L., Campuzano, S.A., Carbone, M., Cesaroni, C., Cianchini, G., De Franceschi, G., De Santis, A., Di Giovambattista, R., Marchetti, D., Martino, L., Perrone, L., Piscini, A., Rainone, M.L., Soldani, M., Spogli, L. and Santoro, F.: Geosystemics View of Earthquakes, Entropy2019,21, 412; doi:10.3390/e21040412, 2019a.

De Santis, A.; Marchetti, D.; Spogli, L.; Cianchini, G.; Pavón-Carrasco, F.J.; Franceschi, G.D.; Di Giovambattista, R.; Perrone, L.; Qamili, E.; Cesaroni, C.; De Santis, A.; Ippolito, A.; Piscini, A.; Campuzano, S.A.; Sabbagh, D.; Amoruso, L.; Carbone, M.; Santoro, F.; Abbattista, C.; Drimaco, D.: Magnetic Field and Electron Density Data Analysis from Swarm Satellites Searching for Ionospheric Effects by Great Earthquakes: 12 Case Studies from 2014 to 2016. Atmosphere 2019, 10, 371, 2019b.

https://doi.org/10.5194/nhess-2019-295
Preprint. Discussion started: 28 November 2019
© Author(s) 2019. CC BY 4.0 License.

Natural Hazards and Earth System Sciences
Discussions

Dobrovolsky I.R., Zubkov S.I. and Myachkin V.I..: Estimation of the size of earthquake preparation zones. Pure Appl. Geophys. Volume 117, Issue 5, pp1025–1044. doi:10.1007/BF00876083, 1979.

Eshelby, J. D.: The determination of the elastic field of an ellipsoidal inclusion, and related problems, Proc. R. Soc. Lond. A. Math. Phys. Sci., 376–396, doi:10.1098/rspa.1983.0054, 1957.

Freund, F.: Rocks That Crackle and Sparkle and Glow: Strange Pre-Earthquake Phenomena. Journal of Scientic Exploration, Vol. 17, No. 1, pp. 37–71, 2003.

Gutenberg, B. and Richter, C. F.: Frequency of earthquakes in California, B. Seismol. Soc. Am., 34, 185–188, 1944.

Hanks, T. C. and Kanamori, H.: A moment magnitude scale, J. Geophys. Res., 84, 2348–2350, https://doi.org/10.1029/JB084iB05p02348, 1979

Luttrell, K. M., Tong, X., Sandwell, D.T., Brooks, B.A. and Bevis, M.G.: Estimates of stress drop and crustal tectonic stress from the 27 February 2010 Maule, Chile, earthquake: Implications for fault strength, J. Geophys. Res., 116, B11401, doi:10.1029/2011JB008509, 2011.

Maksymowicz, A.: The geometry of the Chilean continental wedge: Tectonic segmentation of subduction processes off Chile. Tectonophysics 659 (2015) 183–196, doi: 10.1016/j.tecto.2015.08.007, 2015.

Marchetti, D. and Akhoondzadeh, M.: Analysis of Swarm satellites data showing seismo-ionospheric anomalies around the time of the strong Mexico (Mw = 8.2) earthquake of 08 September 2017. Advances in Space Research 62 (2018) 614–623, https://doi.org/10.1016/j.asr.2018.04.043, 2018.

Marone, C. J. and Saffer, D.M.: The Mechanics of Frictional Healing and Slip Instability During the Seismic Cycle, Treatise on Geophysics: Second Edition, 4 , pp. 111-138. DOI: 10.1016/B978-0-444-53802-4.00092-0, 2015.

Nielsen, S., Spagnuolo, E., Violay, M., Smith, S., Di Toro, G. and Bistacchi, A.: G: Fracture energy, friction and dissipation in earthquakes. J. Seismol. (2016) 20:1187–1205, DOI 10.1007/s10950-016-9560-1, 2016.

Papangelo, A., Ciavarella, M. and Barber, J. R.: Fracture mechanics implications for apparent static friction coefficient in contact problems involving slip-weakening laws471Proc. R. Soc. A http://doi.org/10.1098/rspa.2015.0271, 2015.

https://doi.org/10.5194/nhess-2019-295
Preprint. Discussion started: 28 November 2019
© Author(s) 2019. CC BY 4.0 License.

Parlitz, U., Hornstein, A., Engster, D., Al-Bender, F., Lampaert, V., Tjahjowidodo, T., Fassois, S.D., Rizos, D., Wong, C.X., Worden, K. and Manson, G.: Identification of pre-sliding friction dynamics, Chaos 14, 420–430 (2004). https://doi.org/10.1063/1.1737818, 2004.

Potirakis, S.M., Contoyiannis, Y., Asano, T. and Hayakawa, M.: Intermittency-induced criticality in the lower ionosphere prior to the 2016 Kumamoto earthquakes as embedded in the VLF propagation data observed at multiple stations. Tectonophysics, 722, 422-431. 2018a.

Potirakis, S.M., Asano, T. and Hayakawa, M.: Criticality Analysis of the Lower Ionosphere Perturbations Prior to the 2016 Kumamoto (Japan) Earthquakes as Based on VLF Electromagnetic Wave Propagation Data Observed at Multiple Stations. Entropy 2018, 20, 199; doi: 10.3390/e20030199, 2018b.

Saltas V., Vallianatos F., Triantis D. and Stavrakas I.: Complexity in Laboratory Seismology. Complexity of Seismic Time Series, pages 239-273, 2018.

Scott, J.H.: Electrical and Magnetic properties of rock and soil. UNITED STATES DEPARTMENT OF THE INTERIOR GEOLOGICAL SURVEY. USGS Open-File Report 83-915, 1983.

Schekotov, A. and Hayakawa, M.: Seismo-meteo-electromagnetic phenomena observed during a 5-year interval around the 2011 Tohoku earthquake. Physics and Chemistry of the Earth, 85–86, 167-173, http://dx.doi.org/10.1016/j.pce.2015.01.010, 2015.

Shah, K. P.: The Hand Book on Mechanical Maintenance. Practical Maintenance. Compiled by: K P Shah. http://practicalmaintenance.net/?p=1135, 2011.

Sun, N. P., & Mosleh, M.: The Minimum Coefficient of Friction: What Is It? CIRP Annals, 43(1), 491–495. doi:10.1016/s0007-8506(07)62260-4, 1994.

Turcotte, D. L.: Fractals and Chaos in Geology and Geophysics, Cambridge University Press, Second edition, 397 p., 1997.

Tzanis A. and Vallianatos F.: A physical model of electrical earthquake precursors due to crack propagation and the motion of charged edge dislocations, in: Seismo Electromagnetics (Lithosphere–Atmosphere–Ionosphere-Coupling), TerraPub, 2002, pp. 117–130, 2002.

Utada, H., Shimizu, H., Ogawa, T., Maeda, T., Furumura, T., Yamamoto, T., Yamazaki, N., Yoshitake, Y. and Nagamachi, S.: Geomagnetic field changes in response to the 2011 off the Pacific Coast of Tohoku earthquake and tsunami, Earth Planet. Sci. Lett., 311, 11–27, doi:10.1016/j.epsl.2011.09.036, 2011.

https://doi.org/10.5194/nhess-2019-295
Preprint. Discussion started: 28 November 2019
© Author(s) 2019. CC BY 4.0 License.

Natural Hazards and Earth System Sciences
Discussions

Vallianatos, F. and Tzanis, A.: Electric Current Generation Associated with the Deformation Rate of a Solid: Preseismic and Coseismic Signals. Phys. Chem.Earth,Vol. 23, No. 9-10, pp. 933-938, 1998.

Vallianatos, F. and Tzanis, A.: On the nature, scaling and spectral properties of pre-seismic ULF signals. Natural Hazards and Earth System Sciences, 3: 237–242, European Geosciences Union, 2003.

Vallianatos, F. and Triantis, D.: Scaling in Pressure Stimulated Currents related with rock fracture, Physica A, 387, 4940–4946, https://doi.org/10.1016/j.physa.2008.03.028, 2008.

Venegas-Aravena, P., Cordaro, E. G., and Laroze, D.: A review and upgrade of the lithospheric dynamics in context of the seismo-electromagnetic theory, Nat. Hazards Earth Syst. Sci., 19, 1639–1651, https://doi.org/10.5194/nhess-19-1639-2019, 2019.

Vigny, C., Socquet, A., Peyrat, S., Ruegg, J.-C., Metois, M., Madariaga, R., Morvan, S.,Lancieri, M., Lacassin, R., Campos, J., Carrizo, D., Bejar-Pizarro, M., Barrientos, S.,Armijo, R., Aranda, C., Valderas-Bermejo, M.-C., Ortega, I., Bondoux, F., Baize, S.,Lyon-Caen, H., Pavez, A., Vilotte, J.P., Bevis, M., Brooks, B., Smalley, R., Parra, H.,Baez, J.-C., Blanco, M., Cimbaro, S. and Kendrick, E.: The 2010 Mw 8.8 Maule Megathrust Earthquake of Central Chile, monitored by GPS. Science 332,1417–1421, 2011.

Yue, H., Lay, T., Rivera, L., An, C., Vigny, C., Tong, X. and Báez Soto, J.C.: Localized fault slip to the trench in the 2010 Maule, Chile Mw = 8.8 earthquake from joint inversion of high-rate GPS, teleseismic body waves, InSAR, campaign GPS, and tsunami observations, J. Geophys. Res. Solid Earth, 119, 7786–7804, doi:10.1002/2014JB011340, 2014.

https://doi.org/10.5194/nhess-2019-295
Preprint. Discussion started: 28 November 2019
© Author(s) 2019. CC BY 4.0 License.

Natural Hazards and Earth System Sciences
Discussions

Captions Figures

Figure 1: Schematic description of the non-constant uniaxial stresses in presence of a fault with friction coefficient μ and dip angle θ.

Figure 2: Dimensionless representation of normalized first and second temporal change of the uniaxial stress used by Venegas-Aravena et al. (2019). According to De Santis et al. (2019a) the earthquakes occur close to the center of figures. Here it is when $t = t_0 = 10$.

Figure 3: Temporal behavior of the semi brittle-plastic friction coefficient using different parameters. In all the cases it's possible to observe an increase in the friction before earthquake (t = 10). However, the friction decrease after the earthquake only if k_2 and k_4 has values of $\sim 10^{-9}$.

Figure 4: Schematic description of friction gradient on the fault. When a constant and non-constant temporal stress change is applied at different paces within the lithosphere, a non-zero friction coefficient gradient is expected.

Figure 5: Total fiction coefficient from the Seismo-electromagnetic Theory derivation. If we consider one point within the rupture area, the highest values of friction is found before the earthquake (t = 10). The friction decrease at t=10 was calculated using the stress drop in function of the co-seismic magnetic field. The maximum value is not completely recovery after the earthquake occur.

Figure 6: Schematic comparison among different friction behaviors related with seismic rupture area. Above the result of friction in the context of The Seismo-electromagnetic Theory is presented. At the bottom the classical view of the friction. When the rupture occur, de friction drop is observed in the two theories. However, exist a friction increase in the case studied in this work.

Figure 7: Spatial distribution of γ and γ_2. This functions represent the different sections (or behavior) of friction on the fault along x-direction. The distribution γ_2 represent the stress drop section and distribution γ represent the semi brittle-plastic influence region.

Figure 8: Spatial-temporal Total Friction Coefficient $\bar{\mu}_T(x,t)$ along fault x-direction using $k_2 = k_4 = 10^{-9}$, and the right color bar indicate the friction coefficient values at a certain time and position. The earthquake occur when $t = 10$. At this time, the stress drop (defined by the distribution γ_2) $\Delta\tau \in [8,12]$.

Figure 9: Same spatial-temporal Total Friction Coefficient, however, using $k_2, k_4 = 10^{-10}$.

Figure 10: Total Friction Coefficient using no semi brittle-plastic contribution. That is $\gamma(x) = 0, \forall x \in [0,2x_{half}]$. The friction variation exist only when the earthquake occur ($t = 10$) and at the earthquake rupture place ($\Delta\tau \in [8,12]$ in this case).

Figure 11: Above: The b-value using $\sigma = \alpha\,\tau$; $k_2 = k_4 = 10^{-9}$ and $\alpha = 0.01$. Bottom: The Gutenberg-Richter Law for instants time $t = 0, t = 9$ and $t = 20$. The b-value decreases before the earthquake implying stronger seismic events.

Figure 12: The b-value and Gutenberg-Richter Law using $k_2 = k_4 = 10^{-10}$. The green and red curves are the same.

Figure 13: Different rupture's time viewed from the differential total friction coefficient $d\bar{\mu}_T$ and using different values of k_2 and k_4. The rupture occurs after the maximum differential total friction coefficient $(d\bar{\mu}_T)_{MAX}$, when $d\bar{\mu}_T$ have values close to 0.5-0.9 times $(d\bar{\mu}_T)_{MAX}$.

https://doi.org/10.5194/nhess-2019-295
Preprint. Discussion started: 28 November 2019
© Author(s) 2019. CC BY 4.0 License.

Natural Hazards and Earth System Sciences
Discussions
Open Access
EGU

Figure 1

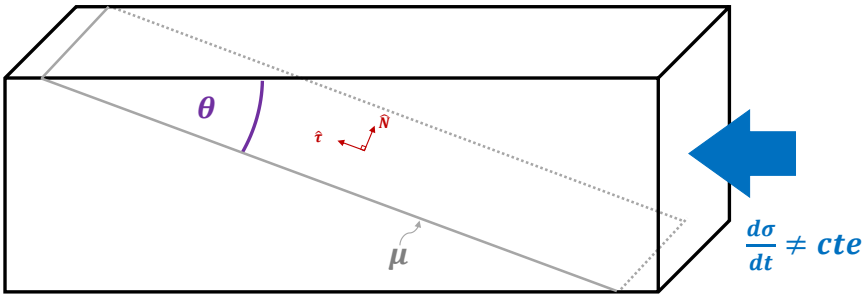

https://doi.org/10.5194/nhess-2019-295
Preprint. Discussion started: 28 November 2019
© Author(s) 2019. CC BY 4.0 License.

Natural Hazards and Earth System Sciences
Discussions
Open Access
EGU

1 Figure 2

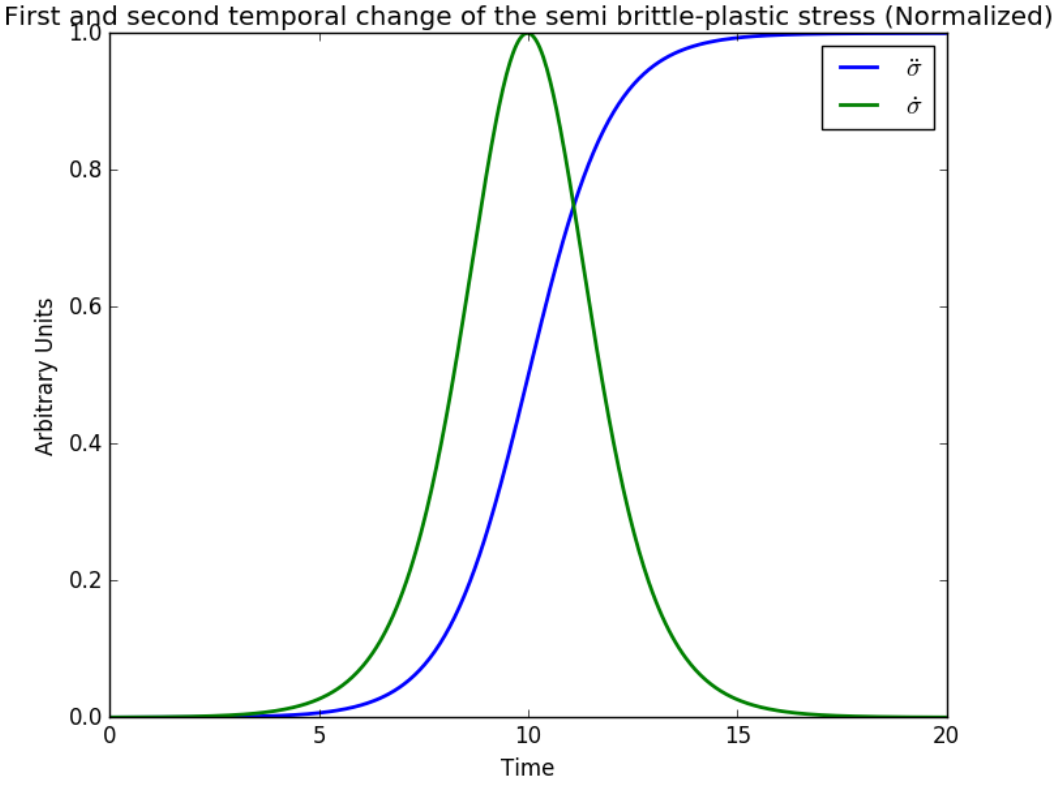

2

3

https://doi.org/10.5194/nhess-2019-295
Preprint. Discussion started: 28 November 2019
© Author(s) 2019. CC BY 4.0 License.

Natural Hazards and Earth System Sciences
Discussions
Open Access
EGU

Figure 3

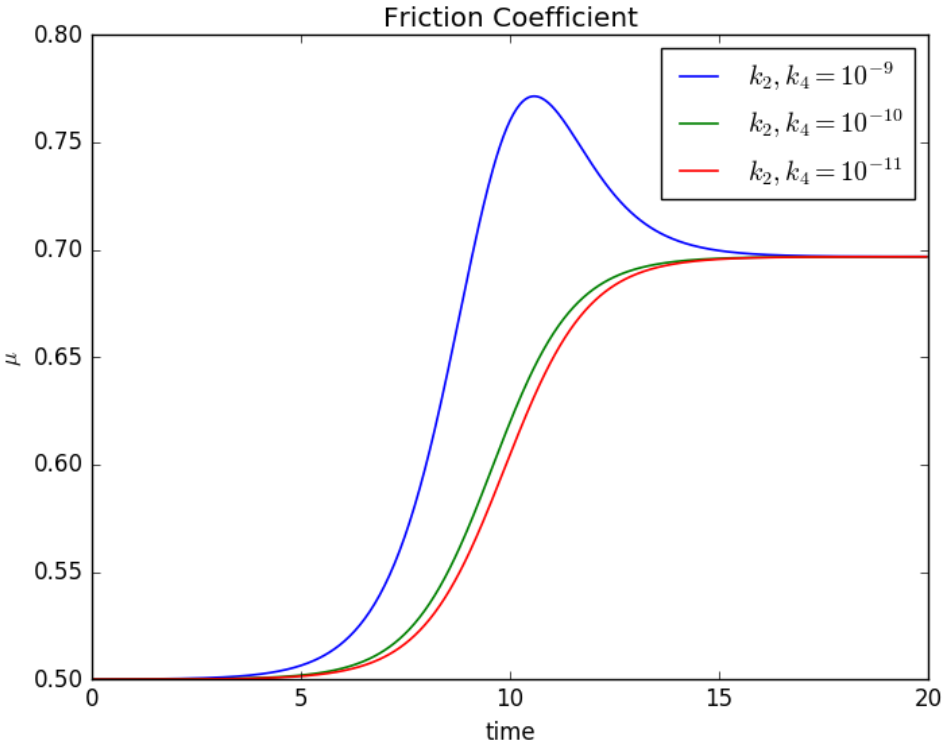

https://doi.org/10.5194/nhess-2019-295
Preprint. Discussion started: 28 November 2019
© Author(s) 2019. CC BY 4.0 License.

Figure 4

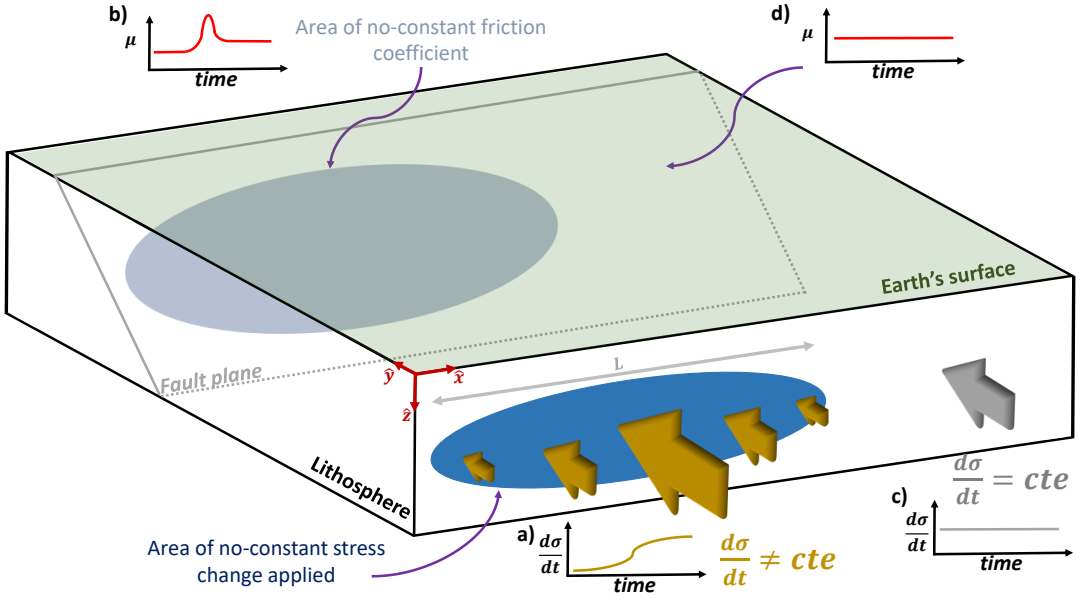

https://doi.org/10.5194/nhess-2019-295
Preprint. Discussion started: 28 November 2019
© Author(s) 2019. CC BY 4.0 License.

Natural Hazards and Earth System Sciences
Discussions
Open Access
EGU

1 Figure 5

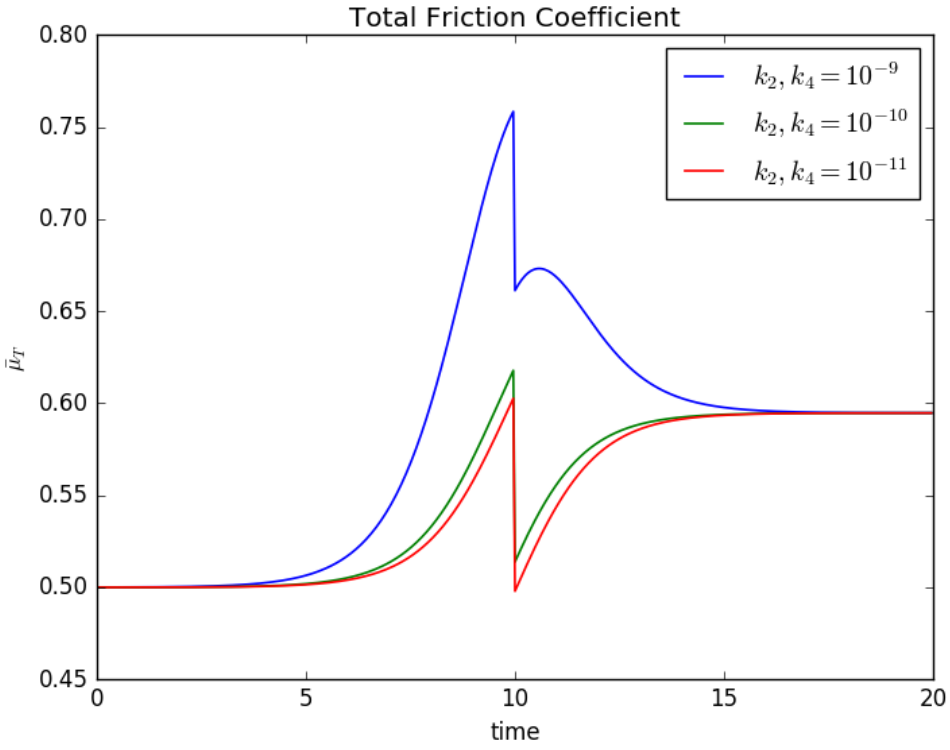

2

3

4

https://doi.org/10.5194/nhess-2019-295
Preprint. Discussion started: 28 November 2019
© Author(s) 2019. CC BY 4.0 License.

Natural Hazards and Earth System Sciences
Discussions
Open Access
EGU

Figure 6

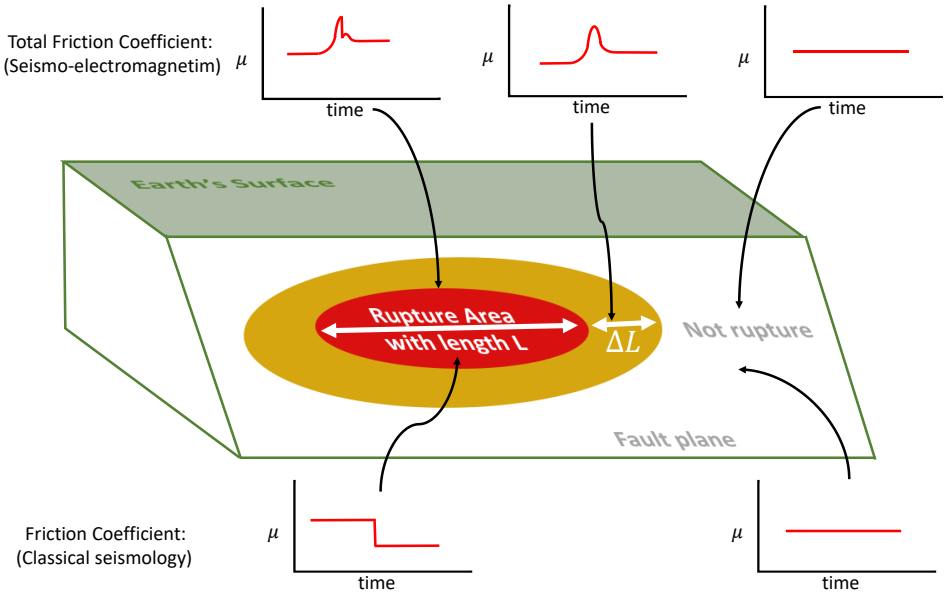

https://doi.org/10.5194/nhess-2019-295
Preprint. Discussion started: 28 November 2019
© Author(s) 2019. CC BY 4.0 License.

Natural Hazards and Earth System Sciences
Discussions
Open Access
EGU

Figure 7

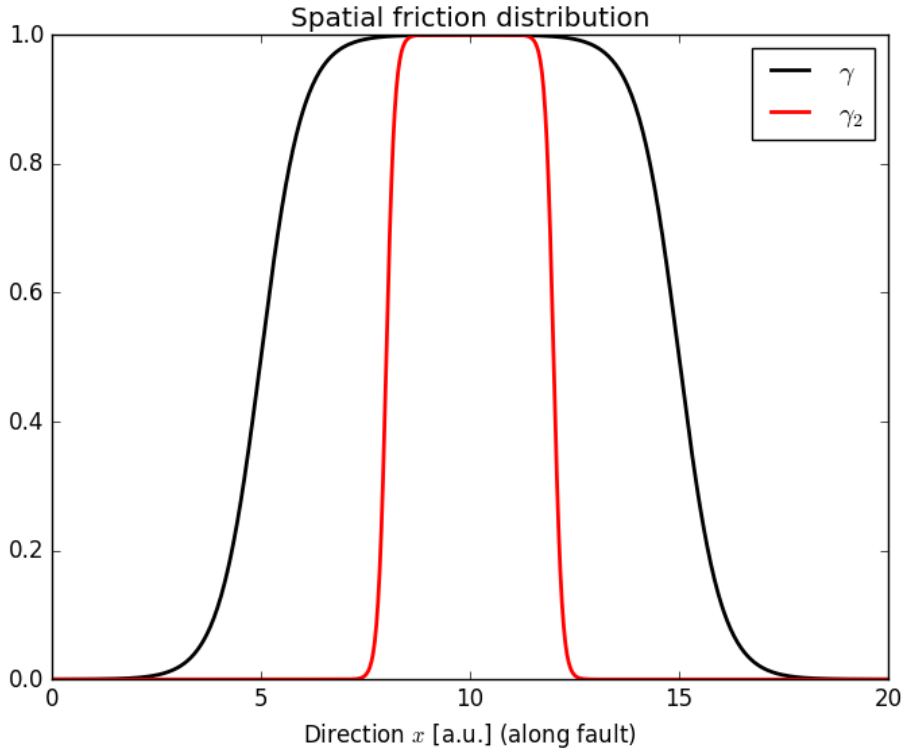

https://doi.org/10.5194/nhess-2019-295
Preprint. Discussion started: 28 November 2019
© Author(s) 2019. CC BY 4.0 License.

Natural Hazards and Earth System Sciences
Discussions
Open Access
EGU

1 Figure 8

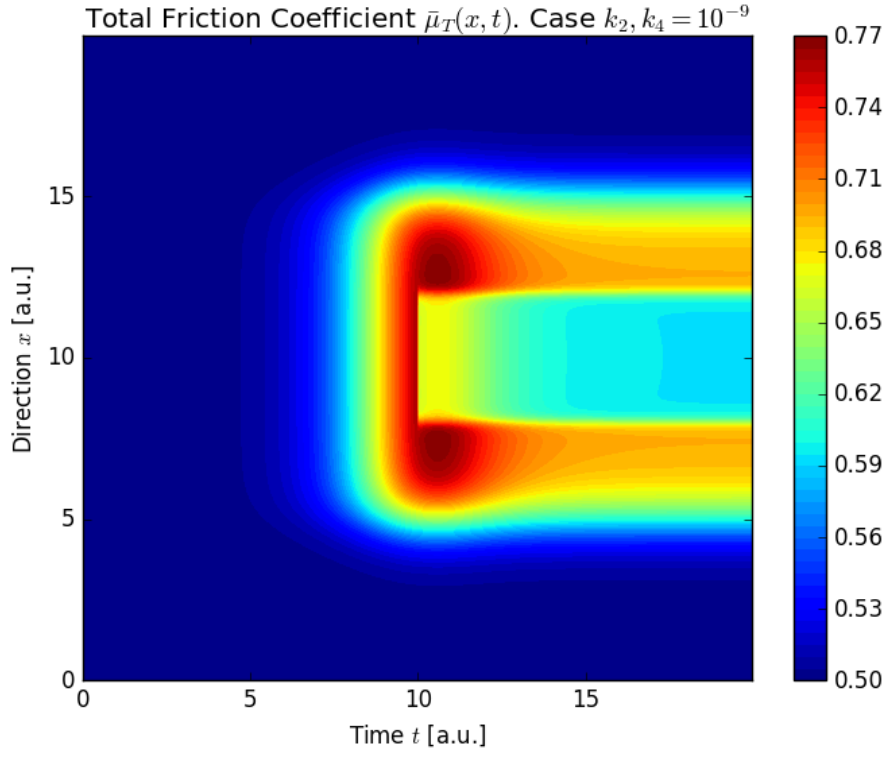

2

https://doi.org/10.5194/nhess-2019-295
Preprint. Discussion started: 28 November 2019
© Author(s) 2019. CC BY 4.0 License.

Natural Hazards and Earth System Sciences
Discussions
Open Access
EGU

Figure 9

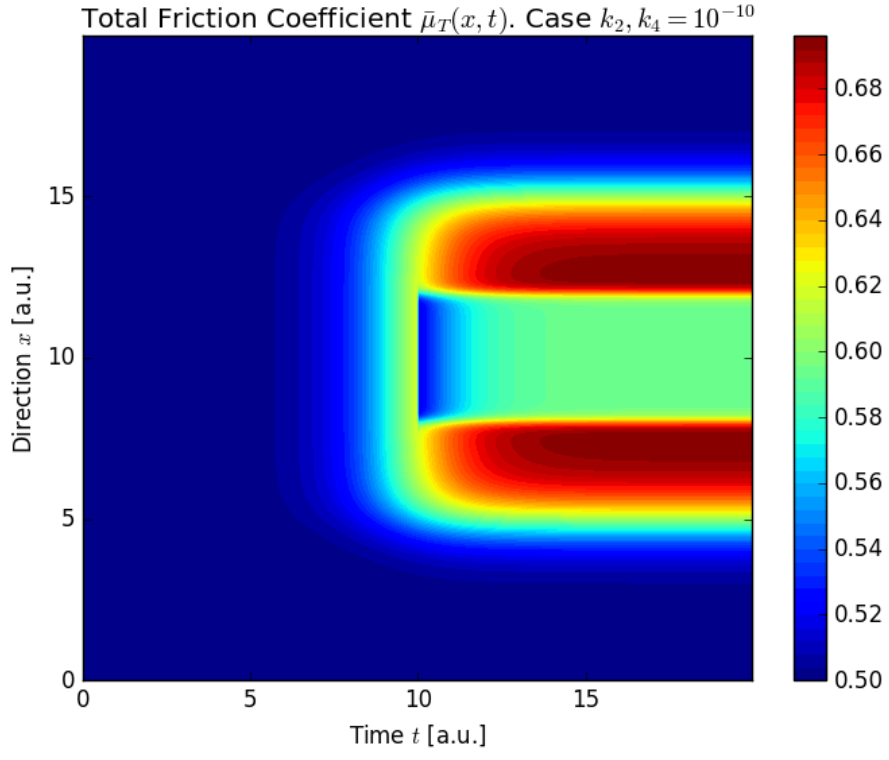

https://doi.org/10.5194/nhess-2019-295
Preprint. Discussion started: 28 November 2019
© Author(s) 2019. CC BY 4.0 License.

Natural Hazards and Earth System Sciences
Discussions
Open Access
EGU

1 Figure 10

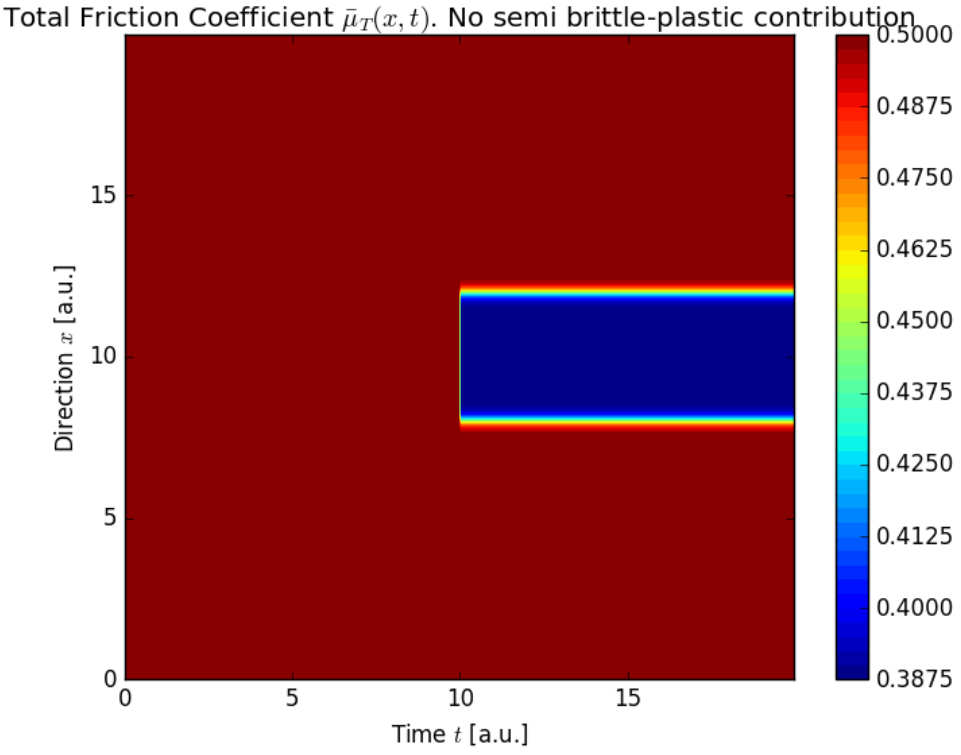

2

https://doi.org/10.5194/nhess-2019-295
Preprint. Discussion started: 28 November 2019
© Author(s) 2019. CC BY 4.0 License.

Natural Hazards and Earth System Sciences
Discussions

Figure 11

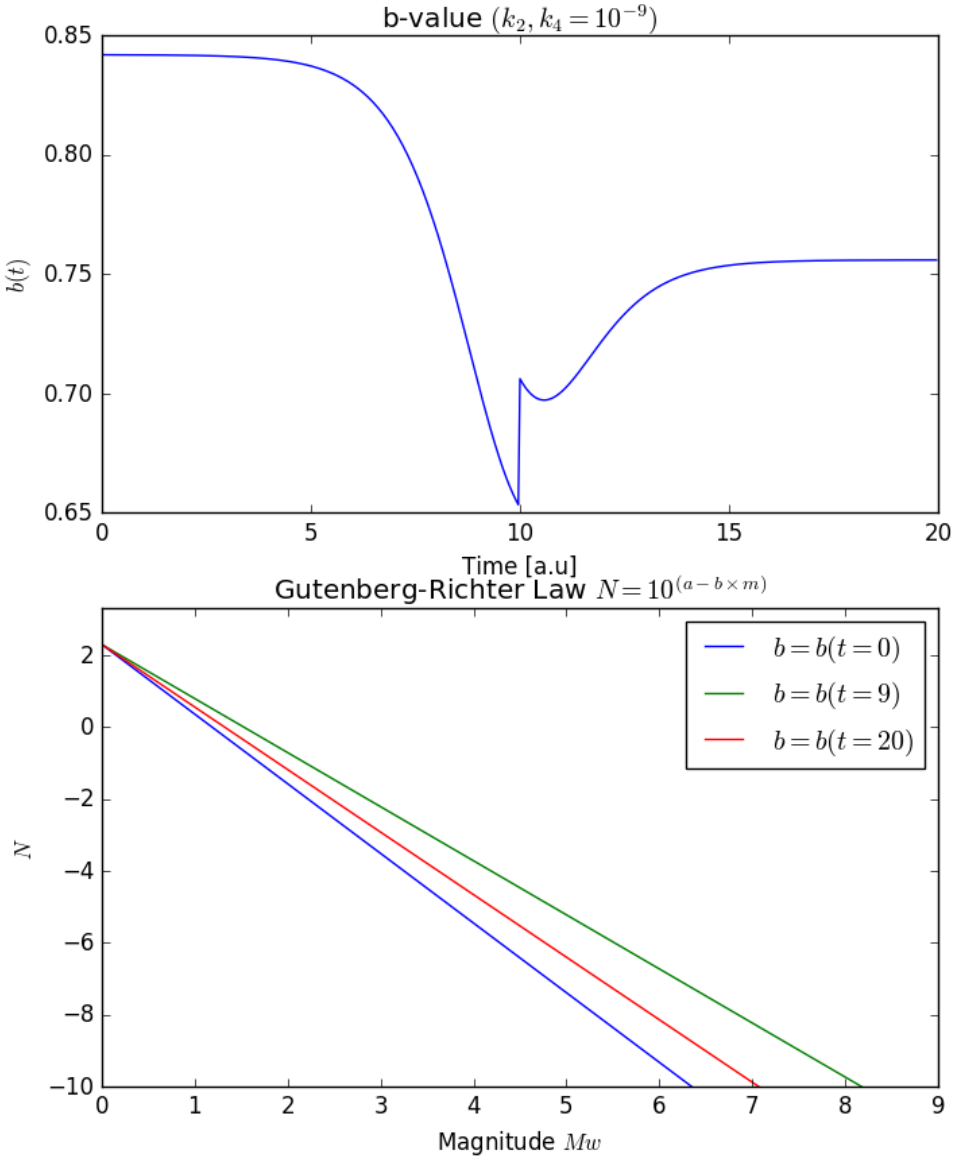

https://doi.org/10.5194/nhess-2019-295
Preprint. Discussion started: 28 November 2019
© Author(s) 2019. CC BY 4.0 License.

Natural Hazards and Earth System Sciences
Discussions
Open Access
EGU

Figure 12

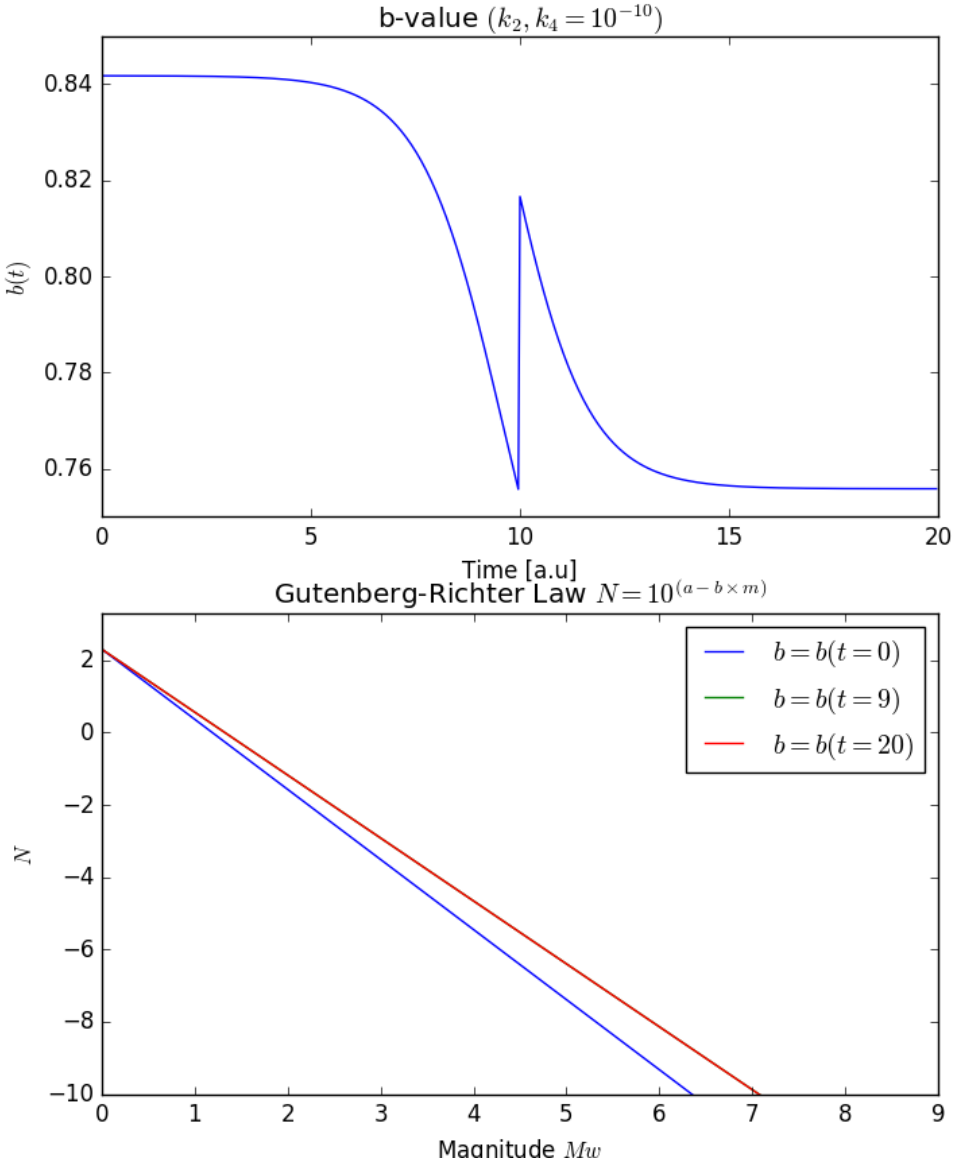

https://doi.org/10.5194/nhess-2019-295
Preprint. Discussion started: 28 November 2019
© Author(s) 2019. CC BY 4.0 License.

Natural Hazards and Earth System Sciences
Discussions
Open Access
EGU
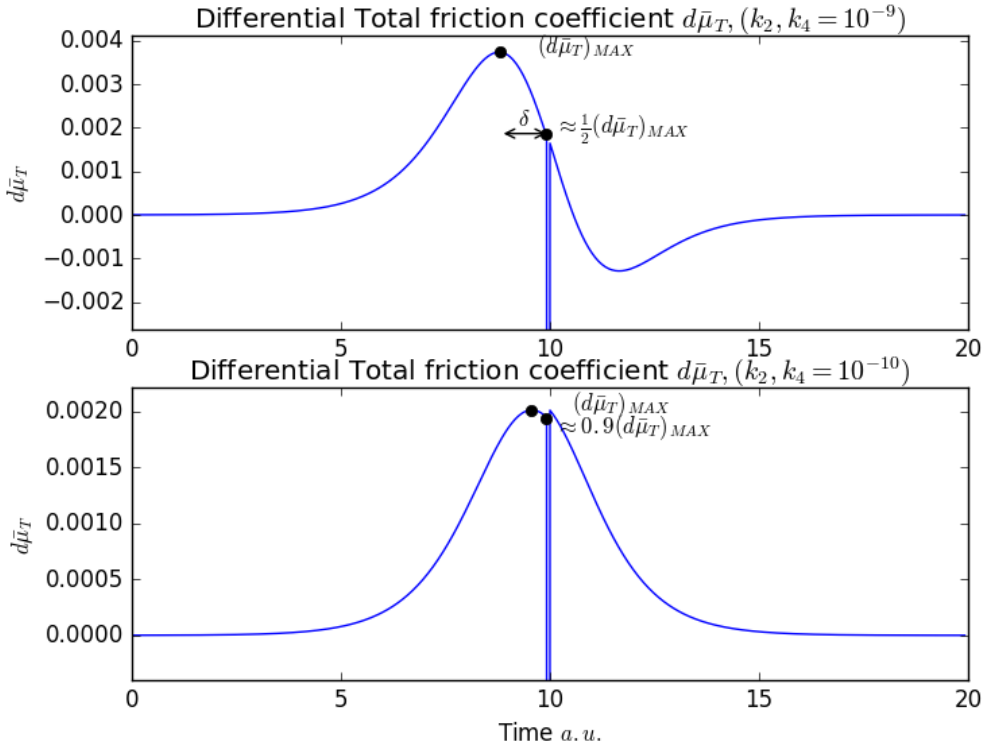
Figure 13